

## Electronic effects in scanning tunneling microscopy of graphite: A Green's-function calculation based on the tight-binding model

B. A. McKinnon

*Department of Physics and Astronomy, University College, London, Gower Street, WC1E 6BT London, United Kingdom*

T. C. Choy

*Department of Physics, Monash University, Clayton, 3156 Australia*

(Received 27 March 1996; revised manuscript received 12 June 1996)

We show that the features of the scanning-tunneling-microscopy STM images of graphite can be understood within a simple tight-binding model of the tip-surface system. Using Green's-function techniques, we are able to go beyond the usual Tersoff and Hamann formalism and include the effect of the bias voltage and tip-surface coupling on the tunneling current. We show that the tunneling current is very sensitive to the different crystallographic stacking arrangements of graphite, due to their influence on the local density of states both at and near the Fermi level. In addition, we find that the relative corrugation of the STM image depends strongly upon the nature of the tip-surface interaction. We conclude with a discussion of the extension of our formalism to include surface defects and adsorbates. [S0163-1829(96)01539-1]

### I. INTRODUCTION

The invention of the scanning tunneling microscope<sup>1</sup> has led to a wealth of exciting observations of surface electronic structure. The case of graphite is no exception and, due to its simple surface structure, provides a useful testing ground for theoretical models. Most models of scanning-tunneling microscopy (STM) are based on that of Tersoff and Hamann,<sup>2,3</sup> in which the tunneling current is found to be proportional to the Fermi level surface density of states at the point probed by the tip. The inequivalent local density of states (LDOS) of the graphite surface sites leads to the resolution of only every second atom under normal tunneling conditions. However, the simple Tersoff and Hamann model explains neither the decrease of resolution with increasing bias voltage in the constant current tunneling mode, nor the decrease in resolution with decreasing tunneling current.<sup>4</sup> In addition there have been observations<sup>5,6(a),6(b)</sup> of changes in the relative corrugation of the image, which also cannot be explained within the Tersoff and Hamann model.

Graphite consists of weakly bound hexagonal lattice layers. While 82% of naturally occurring graphite is of the Bernal form (*ABAB* stacking), 12% of graphite is of the rhombohedral form (*ABCABC* stacking).<sup>7</sup> Frequently a synthetic preparation highly oriented pyrolytic graphite (HOPG) is used, in which the hexagonal carbon lattice layers, while well ordered along the *c* axis, are randomly stacked with respect to the *a* axis. STM of HOPG has revealed a large variety of superlattice structures. While one source of such images is the formation of more than one tip point,<sup>8</sup> allowing tunneling to multiple points on the tip, Moiré patterns<sup>9,10</sup> have also been observed. We shall show that the LDOS close to the Fermi level is particularly sensitive to the interlayer stacking, affecting the tunneling current sufficiently for a "superlattice" structure to be superimposed upon the usual graphite image. The amplitude of the Moiré patterns observed in constant current mode decreases with increasing

bias voltage,<sup>9</sup> which we also find to be consistent with our model.

In constant current mode the tip height is adjusted to maintain a constant tunneling current as the surface is raster scanned. However the observed tip-height corrugation is far greater than that simply due to the distance dependence of the electronic tip-surface matrix element.<sup>11</sup> Because of the proximity of the tip to the surface, the tip exerts a force on the surface, causing it to deform. Since the tip-height corrugation is measured with respect to the back of the sample, the elastic deformation of the surface amplifies the response of the tip driver to the change in the tip-surface tunneling matrix element. The observed Moiré patterns have also been attributed to the variation in tip-surface force resulting from the variable interlayer stacking;<sup>12</sup> however, we show that the bias voltage dependence of the results is more consistent with response to variation in local electronic structure.

As a point probe of real-space surface structure, STM presents significant theoretical challenges, requiring knowledge of the electronic structure of both the tip and surface as well as the nature of the tip-surface interaction. The first model by Tersoff and Hamann<sup>2</sup> employed a first-order perturbation theory tunneling Hamiltonian approach, using the Bardeen approximation for the tunneling matrix element. By assuming an asymptotically spherical tip and taking the limit of small applied bias voltage, the tunneling current was reduced to the Fermi level LDOS of the surface at the point probed by the tip. Subsequently, Tomanek *et al.*<sup>13</sup> demonstrated the need to go beyond the small bias limit to explain the observed bias-dependent, asymmetric images of graphite. The tunneling current can also be calculated nonperturbatively by numerically solving the Schrödinger equation and hence obtaining the current density.<sup>14-17</sup> However, studies comparing the two approaches show good agreement up to tip-surface separations of an Å.<sup>16</sup> Doyen<sup>18</sup> proved that the current-density approach is in fact equivalent to the transfer Hamiltonian method taken to all orders in the tip-surface coupling. More sophisticated calculations also include the

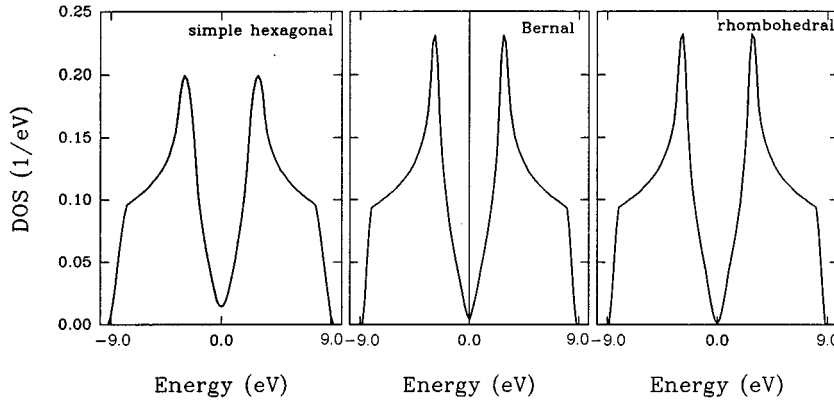


FIG. 1. Surface DOS for (i) simple hexagonal (ii) Bernal and (iii) rhombohedral graphite. (Energy is measured with respect to the Fermi level.)

effect of the image charge on the effective tip-surface potential, which has been shown to further increase the magnitude of the tunneling current.<sup>19,16</sup> A nonequilibrium Green's-function approach was introduced by Sacks and Noguera,<sup>20</sup> involving matching of the tip and sample surface Green's-functions to obtain the tip-sample propagator. Nevertheless for the cases considered so far this approach reduces to conventional Green's function methods such as that in Ref. 21.

One of the most difficult aspects of STM is the problem of reproducibility of tip and tip-surface interactions. The importance of going beyond an  $s$ -like tip has been recognized by many studies.<sup>22–25,5</sup> The STM tip is usually made of platinum or tungsten, allowing for the possibility of tunneling from  $d$ -like and/or  $p$ -like states. Tekman and Ciraci<sup>26</sup> proposed that tip-induced surface states would account for the large observed tip-height corrugations. However, using Green's-function techniques, Doyen, Drakova, and Scheffler<sup>27</sup> investigated such states for Al(111) and found that, while the tip influenced the surface electronic structure, the resultant electronic contribution to the tip-height corrugation in constant current mode was still only of order 0.1 Å compared to the experimentally observed 0.8 Å.

In this work we study the STM of graphite using the tight-binding Hamiltonian (TBH) method to describe the tip-surface system. While more sophisticated electronic structure calculations can provide greater overall accuracy, a TB approach has the advantage of allowing relatively simple elucidation of the important contributions to the STM image. In addition the TB Hamiltonian gives a good description of the electronic structure of graphite near the Fermi level, precisely the regime probed by STM.<sup>28</sup> By using a simple TB model of the graphite-tip system, we are able to demonstrate the extreme sensitivity of the STM image to the form of the tip-surface interaction as well as the applied bias voltage. Our results are an improvement upon previous TB models,<sup>29–31</sup> which employ the small bias limit, and are therefore unable to account for bias voltage effects. Although we have used a TB model, most appropriate for the region of weak chemical interactions 2–8 Å from the surface, the method can be readily generalized to more sophisticated TB-like schemes such as complete neglect of differential overlap (CNDO).<sup>32</sup> TB models are also well suited to Green's-function methods, and thus extension to the inclusion of defects or adsorbates.<sup>33</sup>

## II. MODEL

We describe the graphite-STM tip system within the tight-binding Hamiltonian,

$$\mathbf{H} = \sum_i |i\rangle \epsilon_i \langle i| - \sum_{ij} |i\rangle V_{ij} \langle j|, \quad (1)$$

where the basis  $\{|l\rangle\}$  includes all sites in the tip-surface system.  $V_{ij}$  are nonzero for nearest neighbors only, and represent the hopping energy between sites  $i$  and  $j$ , and  $\epsilon_i$  is the on-site energy at site  $i$ . In our model, the tip is a semi-infinite, one-dimensional chain, and the surface a semi-infinite slab of graphite.

### A. Graphite

The electronic structure of graphite about the Fermi level is well described by the TB model. Within the hexagonal lattice layers the carbon atoms participate in  $sp^2$ -hybridized  $\sigma$  bonding, as well as  $\pi$  bonding between the  $2p_z$  orbitals. The interlayer bonding is significantly weaker and less well understood.<sup>34</sup> In our model we obtain the graphite surface by cleaving an infinite crystal into two semi-infinite crystals<sup>35</sup> (see Appendix A).

By calculating the lattice Green's function for graphite, we are able to obtain the DOS. The lattice Green's-function operator is defined in terms of the Hamiltonian as

$$\mathbf{G}(E) = \frac{1}{E\mathbf{I} - \mathbf{H}}. \quad (2)$$

The DOS is then<sup>36</sup>

$$\rho(E) = -\frac{1}{\pi} \text{Im} \lim_{\epsilon \rightarrow 0^+} \text{Tr}[\mathbf{G}(E + i\epsilon)]. \quad (3)$$

Because the interlayer bonding in graphite is comparatively weak, the DOS is dominated by the features of the two-dimensional hexagonal DOS.<sup>37</sup> The most significant effect of the interlayer bonding is to increase the value of the DOS at the Fermi-level from zero to a small but finite value. The exact nature of the Fermi level DOS in bulk graphite and at the surface depends upon the crystallographic stacking, as can be seen in Fig. 1. At the surface of Bernal graphite, cleavage causes the formation of a virtual surface state exactly at the midpoint of the bandwidth, which, being a zero residue pole, contributes no weight to the DOS. It can be ignored in calculating the tunnelling current as we consider the contribution of states above the Fermi level.<sup>38</sup>

The hexagonal lattice can be viewed as two interpenetrating triangular lattices. While in a hexagonal layer every site is equivalent, the asymmetric interlayer coupling in the Ber-

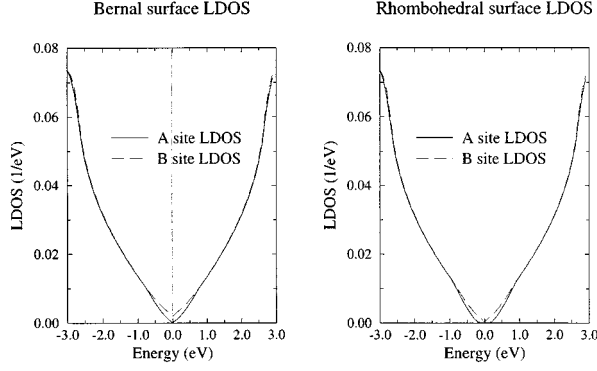


FIG. 2. Resolution of DOS into contributions from  $A$  and  $B$  sites near the Fermi level for (i) Bernal and (ii) rhombohedral graphite.

nal and rhombohedral cases causes the two sites to become inequivalent. We follow convention and refer to the sites with a nearest neighbor in the adjacent plane as the  $A$  site, and the sites situated in the lattice hollows as the  $B$  sites. Due to the electronic inequivalence of the  $A$  and  $B$  sites in Bernal graphite, the LDOS differ about the Fermi level, with the Fermi level LDOS at the  $A$  site being zero while that at the  $B$  site is nonzero. In rhombohedral graphite, the bulk  $A$  and  $B$  sites are equivalent; however, cleavage causes the surface  $A$  and  $B$  sites to become inequivalent. In Fig. 2 it can be seen that, although the Fermi-level LDOS's are both zero, the two LDOS's differ slightly as the Fermi level is approached, leading, as we shall find, to an  $AB$  asymmetry in the STM image.

### B. Tip

The tip is modeled as the final atom of a semi-infinite, one-dimensional chain, for which the Green's function is<sup>39</sup>

$$G(E) = \frac{1}{2W^2} (E \pm \sqrt{E^2 - 4W^2}), \quad (4)$$

where  $W$  is the hopping element between nearest neighbors of the chain. The sign of the square root is determined in order that in the limit that the imaginary part of the energy becomes zero, the DOS is positive [see Eq. (3)].

In Fig. 3 we illustrate our simplified representation of the tip-surface interaction. We have calculated the tunneling current for three extreme cases: tunneling with the tip directly above the  $A$  surface site, tunneling with the tip directly above the  $B$  surface site and tunneling with the tip directly above the center of a hexagon, referred to as the  $H$  site. Electron transfer between the tip and surface is restricted to hopping  $V_1$  from the final tip atom to the nearest-neighbor surface site directly below the tip, and hopping  $V_2$  between the final tip atom and the next-nearest-neighbor site. Although representing the tip-surface interaction in terms of a single atom of a one-dimensional tip with a limited number of surface atoms may seem unrealistic, we shall show that to first order  $V_1$  and  $V_2$  can be equivalently regarded as the sum of all the tip-surface contributions, with contributions from  $A$  and  $B$  sites being separately distinguished.

### C. Tunneling current

We divide the tip-surface Hamiltonian into three parts: one part concerning the tip, the second the surface, and the third the tip-surface interaction, i.e.,

$$\mathbf{H} = \mathbf{H}_{\text{tip}} + \mathbf{H}_{\text{surf}} + \mathbf{H}_{\text{tip-surf}}. \quad (5)$$

$\mathbf{H}_{\text{tip-surf}}$  is treated perturbatively. Within time-dependent perturbation theory, the transition rate between the unperturbed states of the tip  $|\phi_\alpha\rangle$  and those of the surface  $|\phi_\beta\rangle$  can then be written (to all orders in the tip-surface interaction) as

$$W_{\alpha\beta} = \frac{2\pi}{\hbar} |\langle \phi_\alpha | \mathbf{T} | \phi_\beta \rangle|^2 \delta(E_\alpha - E_\beta), \quad (6)$$

where the  $\delta$  function ensures energy conservation and

$$\mathbf{T}(E) = \frac{1}{E\mathbf{I} - \mathbf{G}^0 \mathbf{H}_{\text{tip-surf}}} \mathbf{H}_{\text{tip-surf}}. \quad (7)$$

$\mathbf{G}^0$  is the Green's function of the unperturbed system  $\mathbf{H}_{\text{surf}} + \mathbf{H}_{\text{tip}}$ .

Applying a bias voltage to the tip-surface interface then causes a current to flow,

$$I = \frac{2\pi e}{\hbar} \sum_{\alpha\beta} |\langle \phi_\alpha | \mathbf{T} | \phi_\beta \rangle|^2 \delta(E_\alpha - E_\beta) \times [f(E_\alpha) - f(E_\beta + eV_{\text{bias}})]. \quad (8)$$

Introducing the identity

$$\delta(E_\beta - E_\alpha) = \int_{-\infty}^{\infty} dE \delta(E - E_\alpha) \delta(E - E_\beta), \quad (9)$$

and taking the zero-temperature limit, the current becomes

$$I = \frac{2\pi e}{\hbar} \int_{E_F}^{E_F + eV_{\text{bias}}} dE \sum_{\alpha\beta} \delta(E_\alpha - E) \langle \phi_\alpha | \mathbf{T} | \phi_\beta \rangle \times \langle \phi_\beta | \mathbf{T} | \phi_\alpha \rangle \delta(E_\beta - E), \quad (10)$$

which can be more neatly expressed as<sup>40</sup>

$$I = \frac{2\pi e}{\hbar} \int_{E_F}^{E_F + eV_{\text{bias}}} dE \text{Tr}[\boldsymbol{\rho}_{\text{tip}}(E) \mathbf{T}^\dagger \boldsymbol{\rho}_{\text{surf}}(E) \mathbf{T}], \quad (11)$$

where  $\boldsymbol{\rho}_{\text{tip}}(E)$  and  $\boldsymbol{\rho}_{\text{surf}}(E)$  are the densities of states of the noninteracting tip and surface respectively:

$$\boldsymbol{\rho}_{\text{tip}}(E) = \sum_{\alpha} \delta(E - E_\alpha), \quad (12)$$

$$\boldsymbol{\rho}_{\text{surf}}(E) = \sum_{\beta} \delta(E - E_\beta). \quad (13)$$

We include hopping between the final tip site and the surface site directly below the tip  $V_1$  as well as hopping between the final tip site and the nearest neighbor to the tip on the surface  $V_2$ . As can be seen from Fig. 3, the number of elements summed when calculating the trace is only four with the tip at the  $A$  or  $B$  sites or six with the tip at the  $H$  site. If hopping is allowed between a single tip site and  $n$

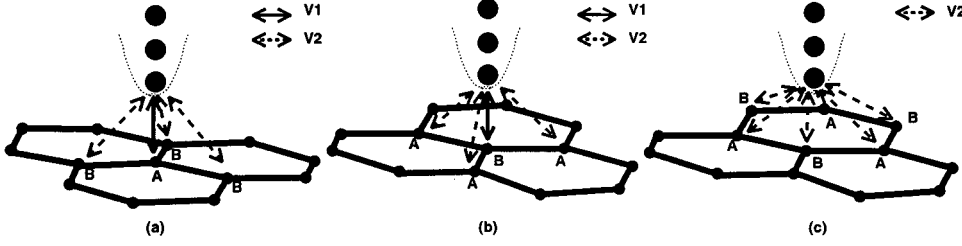


FIG. 3. Representation of the tip-surface interaction with the tip above (a) A, (b) B, and (c) H sites.

surface sites, the elements of  $\mathbf{T}$  linking the tip and the sample have the form [see Appendix B, Eq. (B15)]

$$T_{\text{tip},n} = \frac{V_n}{1 - G_{\text{tip,tip}}^0 \sum_{k,l} V_k V_l G_{kl}^0}, \quad (14)$$

where  $n$  is a surface site from which hopping to the tip,  $V_n$  is allowed and vice versa. The sum over  $k, l$  is over the surface sites involved in tip-surface hopping. Taking the trace, the current becomes

$$I = \frac{2\pi e}{\hbar} \int_{E_F}^{E_F + eV_{\text{bias}}} dE \sum_n \frac{\rho_{nn} \rho_{\text{tip,tip}} V_n^2}{|1 - G_{\text{tip,tip}}^0 \sum_{k,l} V_k V_l G_{kl}^0|^2}. \quad (15)$$

Tip-induced localized states<sup>41</sup> caused by the interaction between the surface and tip are manifested as poles or resonances in the denominator of Eq. (15)<sup>42</sup>

To first order, the current reduces to

$$I = \frac{2\pi e}{\hbar} \int_{E_F}^{E_F + eV_{\text{bias}}} dE \sum_n \rho_{nn} \rho_{\text{tip,tip}} V_n^2, \quad (16)$$

where the sum over  $n$  is over surface sites affected by the tip. Hence the first-order contributions to the tunneling current with the tip at the A, B, and H positions, respectively, become

$$I_A = \frac{2\pi e}{\hbar} \int_{E_F}^{E_F + eV_{\text{bias}}} dE [V_1^2 \rho_A(E) + 3V_2^2 \rho_B(E)] \rho_{\text{tip}}(E), \quad (17a)$$

$$I_B = \frac{2\pi e}{\hbar} \int_{E_F}^{E_F + eV_{\text{bias}}} dE [V_1^2 \rho_B(E) + 3V_2^2 \rho_A(E)] \rho_{\text{tip}}(E), \quad (17b)$$

$$I_H = \frac{2\pi e}{\hbar} \int_{E_F}^{E_F + eV_{\text{bias}}} dE [3V_1^2 \rho_A(E) + 3V_2^2 \rho_B(E)] \rho_{\text{tip}}(E). \quad (17c)$$

The above equations clearly show that if  $V_1^2 > 3V_2^2$ , the current with the tip above the A or B sites will be greater than with the tip at the H position. Because  $\rho_B(E) > \rho_A(E)$  near the Fermi level, the current maxima are observed with the tip at the B site. Minima in the current image occur with the tip above the H position.

For bias voltages smaller than 0.5 eV, the first-order result is indistinguishable from the all orders form of the current, so that the above equations are sufficient to understand the properties of the electronic contribution to STM images.<sup>38</sup>

#### D. Tip-surface matrix element

When the tip is brought close to the surface, the surface potentials of both the tip and surface are perturbed, and the probability of an electron tunneling from the tip to the surface or vice versa, becomes finite. Bardeen<sup>43</sup> showed that, to first order in perturbation theory, the matrix element between two sides of a junction is simply the expectation value of the current operator between the unperturbed wave functions at the interface, i.e.,

$$V_{\alpha\beta} = \frac{\hbar^2}{2m} \int_{\tilde{S}} d\tilde{S} \{ \phi_{\alpha}^{\dagger} \nabla \phi_{\beta} - \phi_{\beta} \nabla \phi_{\alpha}^{\dagger} \}. \quad (18)$$

This is valid if the wave functions both decay exponentially into the vacuum, as is the case in non-contact-mode STM. In our model we approximate the TB tip and surface wave functions by Slater-like  $d_{z^2}$  and  $2p_z$  orbitals, respectively, which clearly decay exponentially with increasing tip-surface separation. Details of these calculations are contained in Appendix C.

### III. RESULTS

#### A. Current imaging mode

We begin by calculating the properties of the tunneling current for constant height operation of the STM. The parameters in the calculation are then the applied bias voltage and the tip-surface hopping parameters  $V_1$  and  $V_2$ . In Fig. 4 we show the dependence of the tunneling current upon the parameter  $V_1$ , which is clearly a function of the tip-surface separation. The applied bias voltage is 0.04 V, and the current is calculated for the tip at positions A, B, and H. The difference between the current that would be obtained from simple hexagonal, Bernal, and rhombohedral forms of graphite is also shown.

From the plots it can be seen that the current is, as would be expected from Eq. (17), quadratic in the tip-surface hopping parameter  $V_1$ . One can also see that the differing LDOS contributions from the A and B sites result in different contributions to the tunneling current. A fascinating difference arises when comparing the case where the secondary hopping contribution  $V_2$  is assumed to be  $0.4V_1$  ( $V_1^2 > 3V_2^2$ ) to that where  $V_2$  is  $0.7V_1$  ( $V_1^2 < 3V_2^2$ ). There is a reversal of the maxima and minima between the two cases. The hollows in the former case are the sites of minimum current, while in the latter case the hollows are the sites of maximum current. Hence the sensitivity of the image to the nature of the tip-surface interaction, as has also been observed experimentally.<sup>5</sup>

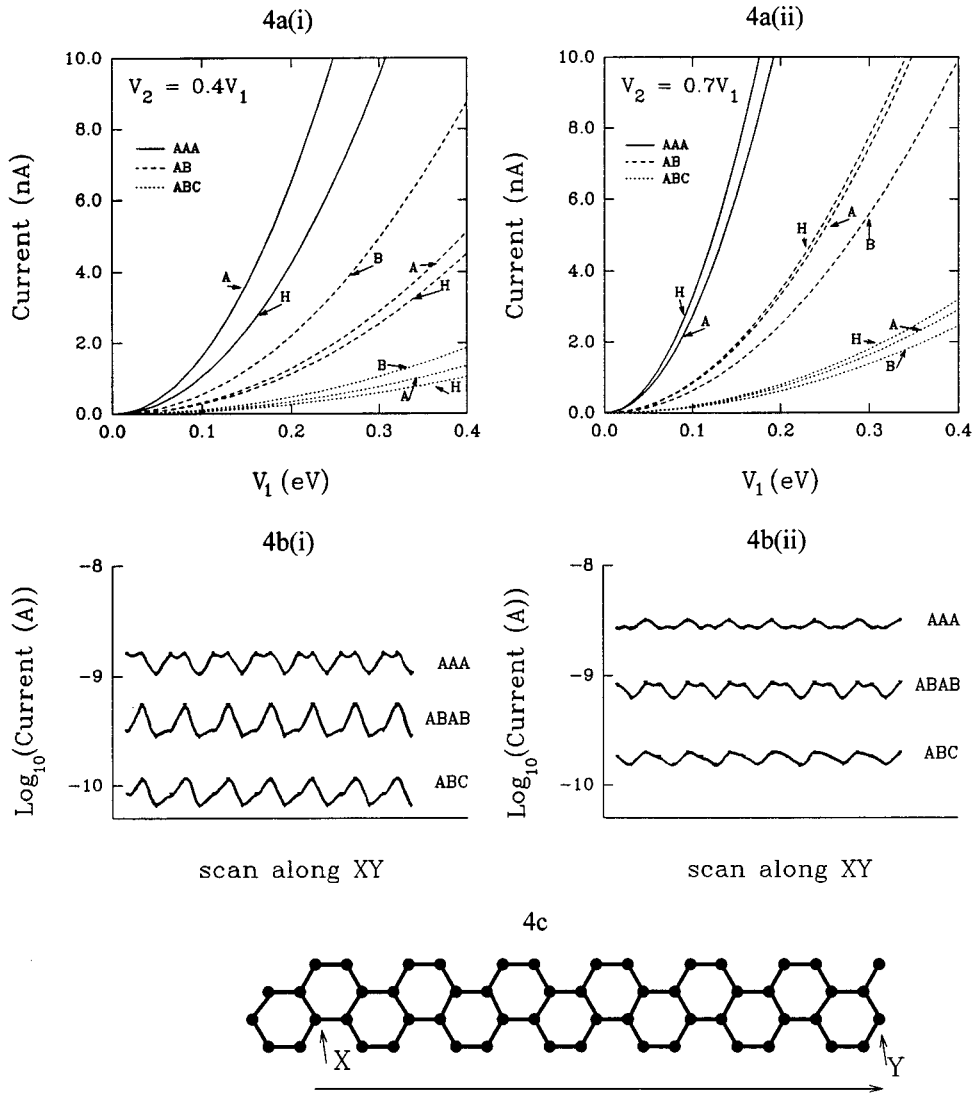


FIG. 4. Current imaging mode of operation of STM: (a) Current as a function of the tip-surface hopping element  $V_1$ . for (i)  $V_2=0.4V_1$  and (ii)  $V_2=0.7V_1$ . (b) Sketch of variation in current for a scan across XY on the graphite surface for cases (i) and (ii). (c) Scan direction across the graphite surface.

This illustration of the sensitivity of the image to the tip-surface interaction is not confined to the case of a point tip interacting with the surface. To first order in the tip-sample interaction,  $V_1$  can equally well represent the sum over the average interaction of *all* the A sites with the tip, and  $V_2$  the sum over the average interaction of *all* the B sites with the tip. In this sense it is unimportant whether the tip is a large cluster, a piece of graphite attached to the tip, or a point source. Such details will affect the magnitude but not the existence of the relative differences in the tunneling current considered here.

An important feature of Fig. 4 is the distinct difference between the magnitudes of the tunneling current from the different forms of graphite. Clearly, in the case of HOPG, the varying interlayer interaction would result in the superposition of a large-scale Moiré pattern upon the underlying atomic scale current variation.

### B. Constant current mode

In constant current mode the height of the STM tip is adjusted so that the measured current remains constant. Modeling this process requires knowledge of both the dependence of the tip-surface hopping parameters upon the tip-

surface separation and the mechanical response of the surface to the tip. In the following we shall ignore the mechanical response (which serves to amplify the change in tip position required to give the necessary change in tip-surface hopping element), and assume that the tip-surface hopping element has the form of Eq. (18), derived by Bardeen.<sup>43</sup>

The current is plotted in Fig. 5 as a function of tip-surface separation at the three tip positions A, B, and H, for the three crystallographic forms of graphite. Below the plots, theoretical STM scans are sketched for a current of 1 nA. Once again, it can be seen that the contributions from the three different forms of graphite are quite distinct. When the bias voltage is increased from 0.02 V to 0.5 V, an important change is observed. The larger number of states contributing to the tunneling current leads to an increase in the average tip-surface separation in order to maintain a tunneling current of 1 nA, and hence to a smaller difference between the tip-surface matrix elements at the A, B, and H sites, decreasing the image corrugation.

Interestingly, at large bias voltages, the results from the different crystallographic forms remain quite distinct, although the absolute separation has decreased. This is consistent with the results of Rong and Kuiper,<sup>9</sup> who performed

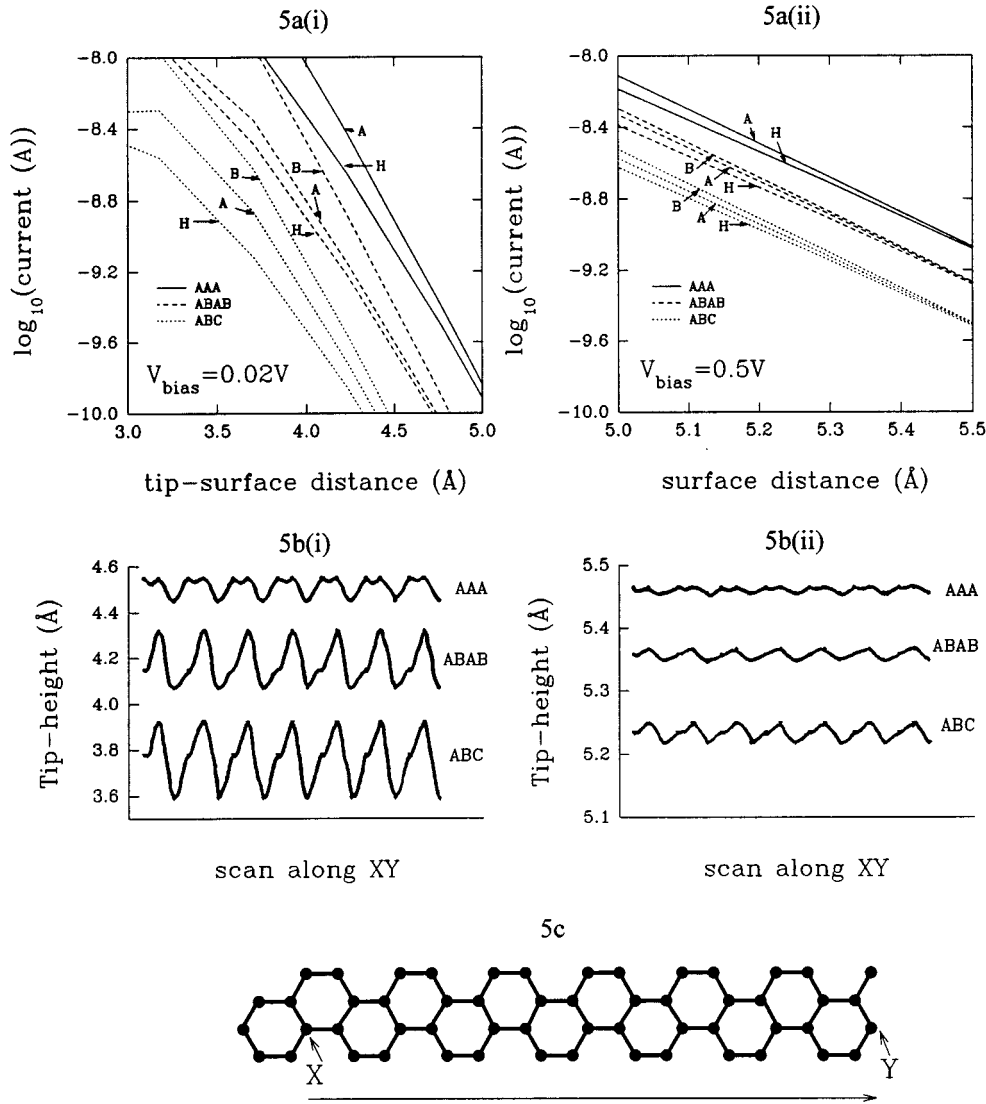


FIG. 5. Constant current mode of operation of STM: (a) Current as a function of the tip-surface separation for (i)  $V_{\text{bias}} = 0.02\text{V}$  and (ii)  $V_{\text{bias}} = 0.50\text{V}$ . (b) Sketch of variation in tip-height for a scan across  $XY$  on the graphite surface for cases (i) and (ii) at a current of 1 nA. (c) Scan direction across the graphite surface.

constant current (5 nA) scans of the surface of HOPG graphite at 0.072 and 0.535 V. They observed a large tip-height corrugation with period 66 Å imposed upon the ordinary atomic scale tip-height corrugation. At a bias voltage of 0.072 V, the large scale tip-height corrugation is 1.8 Å, while the atomic scale tip-height corrugation is 0.6 Å. Increasing the bias voltage to 0.535 V, the atomic scale tip-height corrugation was reduced to 0.4 Å, and the ‘‘superlattice’’ tip-height corrugation to 0.9 Å. That the order of magnitude of the effect is consistent with our results is further indication that the mechanical interaction of tip and the surface serves as a gross amplifier of the response to variations in electronic structure.

#### IV. EXTENSION TO MORE COMPLEX SYSTEMS

The Green’s-function formulation of the tunneling current can readily be extended to more complex surfaces containing defects or adsorbates. Defects or adsorbates at the surface affect the tunneling current in two ways. Both the surface LDOS and tip-surface matrix elements are altered and play a crucial role in interpreting the image.<sup>44</sup> However, given the effect of the adsorbate or defect upon the original surface

Hamiltonian, the new surface LDOS can be explicitly constructed in terms of the old, simplifying the task of calculating the tunneling current.

In calculating the Green’s function of this surface, the adsorbate or defect is treated as a perturbation to the ideal surface. Dyson’s equation then allows the Green’s function of the system to be completely determined in terms of the old Hamiltonian for the system without defect or adsorbate and the perturbation. Here we give the example of an adatom adsorbed onto the  $B$  site of the graphite surface. The ideal surface is perturbed by the on-site energy of the adatom  $\epsilon_\alpha$  and the hopping terms  $W_{i,\alpha}$  from the adatom  $|\alpha\rangle$  to the surface:

$$\mathcal{H} = \mathbf{H} + |\alpha\rangle\epsilon_\alpha\langle\alpha| - \sum_i |i\rangle W_{i,\alpha}\langle\alpha| + \text{H.c.} \quad (19)$$

The sum over  $\{i\}$  is over the atoms interacting with the adatom. The adatom terms constitute a perturbation  $\mathbf{V}$  to the original Hamiltonian so that

$$\mathcal{H} = \mathbf{H} + \mathbf{V} \quad (20)$$

Using Dyson's equation in matrix form, the Green's function and hence the tunneling current [see Eq. (11)] can be obtained for the system:

$$\mathcal{G}_{mn} = G_{mn} + (\mathbf{GVG})_{mn}. \quad (21)$$

Let 0 label the missing or perturbed site and 1, 2, and 3 its nearest neighbors. Dyson's equation becomes

$$\begin{bmatrix} \mathcal{G}_{0n} \\ \mathcal{G}_{1n} \\ \mathcal{G}_{2n} \\ \mathcal{G}_{3n} \end{bmatrix} = \begin{bmatrix} 1 + \epsilon_\alpha G_{00} + \gamma_\alpha(G_{01} + G_{02} + G_{03}) \\ \epsilon_\alpha G_{10} + \gamma_\alpha(G_{11} + G_{12} + G_{13}) \\ \epsilon_\alpha G_{20} + \gamma_\alpha(G_{21} + G_{22} + G_{23}) \\ \epsilon_\alpha G_{30} + \gamma_\alpha(G_{31} + G_{32} + G_{33}) \end{bmatrix} \begin{bmatrix} \gamma_\alpha G_{00} & \gamma_\alpha G_{00} & \gamma_\alpha G_{00} \\ 1 + \gamma_\alpha G_{10} & \gamma_\alpha G_{10} & \gamma_\alpha G_{10} \\ \gamma_\alpha G_{20} & 1 + \gamma_\alpha G_{20} & \gamma_\alpha G_{20} \\ \gamma_\alpha G_{30} & \gamma_\alpha G_{30} & 1 + \gamma_\alpha G_{30} \end{bmatrix} \begin{bmatrix} \mathcal{G}_{0n} \\ \mathcal{G}_{1n} \\ \mathcal{G}_{2n} \\ \mathcal{G}_{3n} \end{bmatrix}. \quad (23)$$

Having solved for  $\mathcal{G}_{0n}$ ,  $\mathcal{G}_{1n}$ ,  $\mathcal{G}_{2n}$ , and  $\mathcal{G}_{3n}$ , they can be substituted back into Eq. (22), and the Green's function of the perturbed system determined.

The Green's function for a system with a perturbation to an A site can be determined in an analogous manner, except now the severing of the interlayer bond must be included, leading to a system of five simultaneous equations.<sup>38</sup>

## V. CONCLUSION

A TB model of the STM of graphite using Green's-function techniques is able to qualitatively describe the experimentally observed features of STM images of graphite. The advantages of this formalism are, first, that the features of the tip-surface interaction are included in a simple and intuitive way; second, that the effect of the bias voltage upon the tunneling current is readily determined; and third, that the effect of the interlayer coupling upon the surface DOS is taken into account. Because we have used Green's-function techniques, our model can be extended to graphite surfaces containing defects or adsorbates. The utility of our method lies in the existence of well-defined TB parameter sets<sup>45</sup> and the popularity of graphite as a substrate for adsorbate studies.

We find that in the case of graphite, the nature of features such as maxima and minima in the STM image are strongly dependent on the tip-surface interaction. In addition, the rapid increase of the DOS away from the Fermi level leads to a high sensitivity of the tunneling current to the nature of the interlayer coupling. We show that this extreme sensitivity suffices to explain Moiré patterns observed at the surface of graphite and is consistent with the experimentally observed bias voltage dependence of the image.

The limitation of TB methods lies in the semiempirical description of the electronic structure of the tip-surface system. For complex geometries, methods such as the recursion technique may be required to obtain the surface Green's function. We plan now to extend the Green's function approach outlined above to general TB-like methods, such as CNDO,<sup>32</sup> where we can take advantage of self-consistent electronic structure calculations in calculating the tunneling current. In addition, through the incorporation of molecular dynamics,<sup>46</sup> we hope to study the dynamic interaction of the

$$\mathcal{G}_{mn} = G_{mn} - [\epsilon_\alpha G_{m0} + \gamma_\alpha(G_{m1} + G_{m2} + G_{m3})]\mathcal{G}_{0n} - \gamma_\alpha G_{m0}(\mathcal{G}_{1n} + \mathcal{G}_{2n} + \mathcal{G}_{3n}), \quad (22)$$

where  $W_{01} = W_{02} = W_{03} = \gamma_\alpha$ . Clearly  $\mathcal{G}_{0n}$ ,  $\mathcal{G}_{1n}$ ,  $\mathcal{G}_{2n}$ , and  $\mathcal{G}_{3n}$  can be solved for self-consistently:

tip and the surface and to model the effect of tip-induced surface deformation on the image. Such methods are necessary in order to adequately model the effects of surface reconstruction and dangling bonds.<sup>47</sup>

## ACKNOWLEDGMENTS

B.A.M. would like to thank the Australian Commonwealth Government for financial support.

## APPENDIX A: CALCULATION OF BULK AND SURFACE GREEN'S FUNCTIONS IN GRAPHITE

The bulk Green's functions for graphite are obtained by determining the expectation value of the Green's-function operator (assuming a nearest-neighbor TB Hamiltonian  $\mathbf{H}$ ),

$$\mathbf{G}^0 = \frac{1}{E\mathbf{I} - \mathbf{H}}. \quad (A1)$$

In graphite, the bulk three-dimensional Green's functions are found to be integrals over complete elliptic integrals of the first kind.<sup>37</sup> The surface Green's functions are obtained in terms of the Green's functions for bulk graphite by exploiting Dyson's equation.<sup>35</sup> A perturbation is applied to the bulk crystal Hamiltonian by removing the hopping term between two layers, creating two surfaces. The Green's function for the divided system can then be obtained in terms of the Green's function for the uncleaved crystal and the perturbation according to Dyson's equation<sup>38</sup>

$$\mathbf{G} = \mathbf{G}^0 + \mathbf{G}^0 \mathbf{V} \mathbf{G}. \quad (A2)$$

Although this appears to involve inversion of an  $N \times N$  matrix equation, because  $\mathbf{V}$  only spans the space of cleaved bonds, the system of equations to be solved reduces to the size of the spanned space. The exact expressions for the surface Green's function for ideally cleaved simple hexagonal, Bernal and rhombohedral graphite may be found in Ref. 38.

## APPENDIX B: TIP-SURFACE MATRIX ELEMENTS

The Hamiltonian of the noninteracting tip-sample system, in block diagonal form, is

$$\mathbf{H}^0 = \begin{bmatrix} \mathbf{H}_{\text{sample}} & 0 \\ 0 & \mathbf{H}_{\text{tip}} \end{bmatrix}, \quad (\text{B1})$$

where  $\mathbf{H}_{\text{sample}}$  is an  $n \times n$  matrix consisting of all the sites in the sample, and  $\mathbf{H}_{\text{tip}}$  is an  $m \times m$  matrix consisting of all the sites in the tip.

In our model, hopping is allowed between the end tip site,  $t$ , and  $l$  surface sites. The Hamiltonian becomes

$$\mathbf{H} = \begin{bmatrix} \mathbf{H}_{\text{sample}} & \mathbf{V} \\ \mathbf{V}^\dagger & \mathbf{H}_{\text{tip}} \end{bmatrix}, \quad (\text{B2})$$

where  $\mathbf{V}$  is a  $m \times n$  matrix, but with the only nonzero elements  $\{V_l\}$  being between the final tip atom and  $l$  surface sites. Dyson's equation gives the Green's function for the whole system in terms of the unperturbed Green's function operator

$$\mathbf{G} = \mathbf{G}^0 + \mathbf{G}^0 \mathbf{T} \mathbf{G}^0, \quad (\text{B3})$$

where

$$\mathbf{T} = \frac{\mathbf{V}}{\mathbf{1} - \mathbf{G}^0 \mathbf{V}}. \quad (\text{B4})$$

Rearranging Eq. (B4) gives

$$\mathbf{T}(\mathbf{1} - \mathbf{G}^0 \mathbf{V}) = \mathbf{V}. \quad (\text{B5})$$

The nonzero matrix elements of  $\mathbf{G}^0 \mathbf{V}$  are

$$(\mathbf{G}^0 \mathbf{V})_{pq} = \begin{cases} \sum_m V_m G_{pm}^0, & q = t \\ V_q G_{pt}^0, & q \in \{l\} \end{cases} \quad (\text{B6})$$

Therefore Eq. (B5) becomes

$$V_j = \sum_i T_{ti} [\delta_{ij} - (G^0 V)_{ij}]. \quad (\text{B7})$$

If  $j$  is the tip site  $t$ , then  $V_{tt} = 0$ , so that

$$0 = T_{tt} - \sum_i T_{ti} (G^0 V)_{it} \quad (\text{B8})$$

$$= T_{tt} - \sum_{ik} T_{ti} V_k G_{ik}^0, \quad (\text{B9})$$

where the sum is over all  $i, k \in \{l\}$ . If  $j \in \{l\}$ , then Eq. (B7) becomes

$$V_j = T_{ij} - T_{it} V_j G_{it}^0. \quad (\text{B10})$$

Substituting Eq. (B10) into Eq. (B9), we obtain

$$0 = T_{tt} - \sum_{ik} (V_i + V_i T_{it} G_{it}^0) V_k G_{ik}^0, \quad (\text{B11})$$

$$\sum_{ik} V_i V_k G_{ik}^0 = T_{tt} \left( 1 - \sum_{ik} V_i V_k G_{it}^0 G_{ik}^0 \right), \quad (\text{B12})$$

$$T_{tt} = \frac{\sum_{ik} V_i V_k G_{ik}^0}{1 - G_{tt}^0 \sum_{ik} V_i V_k G_{ik}^0}. \quad (\text{B13})$$

Putting Eq. (B13) into Eq. (B10),

$$T_{tm} = V_m - V_m G_{tt}^0 \left( \frac{\sum_{ik} V_i V_k G_{ik}^0}{1 - G_{tt}^0 \sum_{ik} V_i V_k G_{ik}^0} \right) \quad (\text{B14})$$

$$= \frac{V_m}{1 - G_{tt}^0 \sum_{ik} V_i V_k G_{ik}^0}. \quad (\text{B15})$$

Looking now at the elements of  $\mathbf{T}$  between surface sites  $m$  and  $n$ , Eq. (B7) becomes

$$0 = \sum_i T_{mi} [\delta_{in} - (\mathbf{G} \mathbf{V})_{in}] \quad (\text{B16})$$

$$= T_{mn} - \sum_i T_{mi} V_n G_{it}^0. \quad (\text{B17})$$

From Eq. (B6), this reduces to

$$0 = T_{mn} - T_{mt} V_n G_{tt}^0. \quad (\text{B18})$$

Hence the elements of  $\mathbf{T}$  between surface sites  $m$  and  $n$  are

$$T_{mn} = \frac{V_n V_m G_{tt}^0}{1 - G_{tt}^0 \sum_{ik} V_i V_k G_{ik}^0}. \quad (\text{B19})$$

### APPENDIX C: TIP-SURFACE HOPPING PARAMETER

In our calculation of the STM tunneling current, we represent the nearest- and next-nearest-neighbor tip-sample hopping terms by the parameters  $V_1$  and  $V_2$ , respectively. In order to estimate the approximate dependence of these parameters upon the tip-surface separation, we have performed the following calculation.

The TB tip-surface hopping parameters are defined by

$$V = \langle \psi_{\text{surf}} | \mathbf{H} | \psi_{\text{tip}} \rangle, \quad (\text{C1})$$

where  $\{\psi_i\}$  are eigenstates of the TBH, the set of Wannier states centered about the lattice sites. However, to calculate  $V$ , we approximate the Wannier states by atomiclike states  $\{\phi_i\}$  which are eigenstates of an atomiclike Hamiltonian, so that

$$V = \int d\tau \phi^*(\vec{r}_{\text{surf}}) \Delta U(\vec{r}) \phi(\vec{r}_{\text{tip}}), \quad (\text{C2})$$

where  $\Delta U(\vec{r})$  is the difference between the atomic potential and the true tip-surface potential. Bardeen<sup>43</sup> showed that Eq. (46) to first order in  $\Delta U(\vec{r})$  is equivalent to

$$V = \int_{\vec{S}} d\vec{S} \cdot \{ \phi^*(\vec{r}_{\text{surf}}) \nabla \phi(\vec{r}_{\text{tip}}) - \phi(\vec{r}_{\text{tip}}) \nabla \phi^*(\vec{r}_{\text{surf}}) \}. \quad (\text{C3})$$

The integration surface is chosen to be the infinite  $x$ - $y$  plane halfway between the tip and the surface. We approximate the Wannier states in graphite by the atomiclike  $2p_z$  wave functions localized about each lattice site. Here we present results for the tip modeled by  $3d_{z^2}$  hydrogenlike wave functions. Reference 38 also contains tip-height corrugation results for a  $1s$ -like and  $2p_z$ -like tips, which show the same overall trends, though with smaller magnitude. In atomic units, the respective wave functions are

$$\phi_{\text{surf}} = \frac{\zeta^{5/2}}{\sqrt{\pi}} z_s e^{-\zeta r_s}, \quad (\text{C4})$$

$$\phi_{\text{tip},d} = \frac{\alpha^{7/2}}{3\sqrt{2\pi}} (3z_t^2 - r_t^2) e^{-\alpha r_t}, \quad (\text{C5})$$

where  $r_s$  is the position vector of the surface wave function, and  $r_t$  is the position vector of the tip wave function.  $\zeta$  and  $\alpha$  correspond to  $Z\gamma/n$ , where  $\gamma$  is a parameter accounting for the screening of the nucleus by the inner electrons,  $Z$  is the atomic number, and  $n$  is the principal quantum number. The corresponding hopping parameters are calculated from

$$V_{\text{dip}} = 13.6 \text{ eV} \frac{\alpha^{7/2} \zeta^{5/2}}{\pi} \int dS e^{-\zeta \bar{r}_s - \alpha \bar{r}_t} d^2 \left[ \frac{7}{4} - \frac{\alpha \bar{r}_t}{4} - \frac{\zeta \bar{r}_t^2}{4 \bar{r}_s} \right. \\ \left. - \frac{\bar{r}_t^2}{d^2} - \frac{3\alpha d^2}{16 \bar{r}_t} - \frac{3\zeta d^2}{16 \bar{r}_s} \right], \quad (\text{C6})$$

where  $\bar{r}_s(\bar{r}_t)$  is  $r_s(r_t)$  evaluated at the surface (tip), and  $d$  is the tip-surface separation. Using MATHEMATICA, we calculated  $V_{\text{dip}}$  as a function of the tip-surface separation assuming  $\alpha = \zeta = 1.5$ . These values are representative of those of the free carbon atom value of  $\zeta = 1.6$ ,<sup>48</sup> and  $\alpha = 1.3$  for a tungsten tip.<sup>49</sup>

- <sup>1</sup>G. Binnig and H. Rohrer, *Helv. Phys. Acta* **55**, 726 (1982).  
<sup>2</sup>J. Tersoff and D. Hamann, *Phys. Rev. Lett.* **50**, 1998 (1983).  
<sup>3</sup>J. Tersoff and D. Hamann, *Phys. Rev. B* **31**, 805 (1985).  
<sup>4</sup>J. Soler, A. Baro, N. Garcia, and H. Rohrer, *Phys. Rev. Lett.* **57**, 444 (1986).  
<sup>5</sup>C. Chen, *J. Vac. Sci. Technol. B* **12**, 2193 (1994).  
<sup>6</sup>(a) P. Ouseph, T. Poothackanal, and G. Mathew, *Phys. Lett. A* **205**, 65 (1995); (b) S. Awo and C. K. Shin, *Phys. Rev. B* **47**, 13 059 (1993).  
<sup>7</sup>R. Haering, *Can. J. Phys.* **36**, 352 (1958).  
<sup>8</sup>H. Mizes, S.-I. Park, and W. Harrison, *Phys. Rev. B* **36**, 4491 (1987).  
<sup>9</sup>Z. Rong and P. Kuiper, *Phys. Rev. B* **48**, 17 427 (1993).  
<sup>10</sup>J. Xhie, K. Sattler, M. Ge, and N. Venkateswaran, *Phys. Rev. B* **47**, 15 835 (1993).  
<sup>11</sup>H. Mamin *et al.*, *Phys. Rev. B* **34**, 9015 (1986).  
<sup>12</sup>M.-H. Whang-bo *et al.*, *J. Phys. Chem.* **98**, 7602 (1994).  
<sup>13</sup>D. Tomanek *et al.*, *Phys. Rev. B* **35**, 7790 (1987).  
<sup>14</sup>N. Lang, *Phys. Rev. B* **36**, 8173 (1987).  
<sup>15</sup>A. Lucas *et al.*, *Phys. Rev. B* **37**, 10 708 (1988).  
<sup>16</sup>T. Laloyaux *et al.*, *Phys. Rev. B* **47**, 7508 (1993).  
<sup>17</sup>X.-W. Liu and A. Stamp, *J. Vac. Sci. Technol. B* **12**, 2189 (1994).  
<sup>18</sup>G. Doyen, *J. Phys. Condens. Matter* **5**, 3305 (1993).  
<sup>19</sup>Z.-H. Huang, M. Weimer, and R. Allen, *Phys. Rev. B* **48**, 15 068 (1993).  
<sup>20</sup>W. Sacks and C. Noguera, *J. Microsc.* **152**, 23 (1988).  
<sup>21</sup>J. Pendry, A. Prêtre, and B. Krutzen, *J. Phys. Condens. Matter* **3**, 4313 (1991).  
<sup>22</sup>W. Sacks and C. Noguera, *Phys. Rev. B* **43**, 11 612 (1991).  
<sup>23</sup>J. Tersoff and N. Lang, *Phys. Rev. Lett.* **65**, 1132 (1990).  
<sup>24</sup>N. Isshiki, K. Kobayashi, and M. Tsukada, *Surf. Sci.* **238**, L439 (1990).  
<sup>25</sup>M. Tsukada, K. Kobayashi, and N. Isshiki, *Surf. Sci.* **242**, 12 (1991).  
<sup>26</sup>E. Tekman and S. Ciraci, *Phys. Rev. B* **40**, 10 286 (1989).  
<sup>27</sup>G. Doyen, D. Drakova, and M. Scheffler, *Phys. Rev. B* **47**, 9778 (1993).  
<sup>28</sup>There is a long history of TB models of graphite. The well-known Slonczewski-Weiss-McClure model [J. Slonczewski and P. Weiss, *Phys. Rev. B* **99**, 636 (1995); J. McClure, *Phys. Rev.* **108**, 612 (1957)] is a popular fourth-nearest-neighbor scheme, although it can be shown [B. McKinnon and T. Choy, *Phys. Rev. B* **52**, 14 531 (1995)] to be equivalent to the nearest-neighbor non-orthogonal TB model.  
<sup>29</sup>D. Tománek and S. Louie, *Phys. Rev. B* **37**, 8327 (1988).  
<sup>30</sup>H. Ou-Yang, B. Källebring, and R. Marcus, *J. Chem. Phys.* **98**, 7405 (1993).  
<sup>31</sup>H. Ou-Yang, B. Källebring, and R. Marcus, *J. Chem. Phys.* **98**, 7565 (1993).  
<sup>32</sup>J. Pople and D. Beveridge, *Approximate Methods in Molecular Orbital Theory* (McGraw-Hill, New York, 1970).  
<sup>33</sup>H. Mizes and J. Foster, *Science* **244**, 559 (1989).  
<sup>34</sup>J.-C. Charlier, X. Gonze, and J.-P. Michenaud, *Europhys. Lett.* **28**, 403 (1994).  
<sup>35</sup>D. Kalkstein and P. Soven, *Surf. Sci.* **26**, 85 (1971).  
<sup>36</sup>E. Economou, *Green's Functions in Quantum Physics*, 2nd ed. (Springer-Verlag, Berlin, 1979).  
<sup>37</sup>B. McKinnon and T. Choy, *Aust. J. Phys.* **46**, 601 (1993).  
<sup>38</sup>B. McKinnon, Ph.D. thesis, Monash University, Australia, 1995.  
<sup>39</sup>E. Foo, M. Thorpe, and D. Weaire, *Surf. Sci.* **57**, 323 (1976).  
<sup>40</sup>An equivalent expression of the tunnelling current is obtained beginning from the equation of motion of the density operator in Refs. 20 and T. Todorov, G. Briggs, and A. Sutton, *J. Phys. Condens. Matter* **5**, 2389 (1993).  
<sup>41</sup>I. Batra and S. Ciraci, *J. Vac. Sci. Technol. A* **6**, 313 (1988).  
<sup>42</sup>This form of the tunneling current is directly related to those obtained employing the nonequilibrium Keldysh formalism such as Refs. 19 and J. Ferrer, A. Martin-Rodero, and F. Flores, *Phys. Rev. B* **38**, 10 113 (1988).  
<sup>43</sup>J. Bardeen, *Phys. Rev. Lett.* **6**, 57 (1961).  
<sup>44</sup>P. Sautet and C. Joachim, *Ultramicroscopy* **42-44**, 115 (1992).  
<sup>45</sup>W. Harrison, *Electronic Structure and Properties of Solids* (Freeman, San Francisco, 1980).  
<sup>46</sup>To carry out this work we intend to modify an existing semi-empirical molecular dynamics scheme, CHEMOS, developed in D. Wallace *et al.*, *J. Phys. Condens. Matter* **3**, 3879 (1991).  
<sup>47</sup>M. Ramos, A. Stoneham, and A. Sutton, *J. Phys. Condens. Matter* **5**, 2849 (1993).  
<sup>48</sup>E. Clementi and L. Roetti, *At. Data Nucl. Data Tables* **14**, 178 (1974).  
<sup>49</sup>F. Zypman, L. Fonseca, and Y. Goldstein, *Phys. Rev. B* **49**, 1981 (1994).